

Correlation and convolution filtering and image processing for pitch evaluation of 2D micro- and nano-scale gratings and lattices

XIAOMEI CHEN^{1,*}, LUDGER KOENDERS², SIMON PARKINSON³

¹Centre for Autonomous & Cyber-Physical System, Cranfield University, Cranfield MK43 0JR, UK

²Surface Metrology Department, Physikalisch-Technische Bundesanstalt(PTB), Bundesallee 100, 38116 Braunschweig, Germany

³School of Computing, University of Huddersfield, Queensgate, HD1 4DH Huddersfield, West Yorkshire, UK

*Corresponding author: xiaomei.chen@cranfield.ac.uk

Received XX Month XXXX; revised XX Month, XXXX; accepted XX Month XXXX; posted XX Month XXXX (Doc. ID XXXXX); published XX Month XXXX

We have mathematically explicated and experimentally demonstrated how a correlation and convolution filter can dramatically suppress the noise that coexists with the scanned topographic signals of 2D gratings and lattices with 2-dimensional (2D) perspectives. To realize pitch evaluation, the true peaks' coordinates have been precisely acquired after detecting the local maxima from the filtered signal, followed by image processing. The combination of 2D filtering, local-maxima detecting and image processing make up the pitch detection (PD) method. It is elucidated that the pitch average, uniformity, rotation angle and orthogonal angle can be calculated using the PD-method. This has been applied to the pitch evaluation of several 2D gratings and lattices, and the results are compared with the results of using the CG- and FT-method. The differences of pitch averages which are produced using the PD-, CG- and FT-methods are within 1.5 pixels. Moreover, the PD-method has also been applied to detect the dense peaks of Si (111) 7×7 surface and the HOPG basal plane. © 2015 Optical Society of America

OCIS codes: (120.0120) Instrumentation, measurement, and metrology; (100.0110) Imaging processing; (070.6110) Spatial filtering; (180.0180) Microscopy.

<http://dx.doi.org/10.1364/AO.99.099999>

NOMENCLATURE

CC	Correlation and convolution; correlation or convolution
XYZ or XOY	3D or 2D coordinates system of sample surface
xyz or xoy	3D/2D coordinates of measuring instrument, e.g. an SPM
φ_x, φ_y	The angles that XOY plane tilts relative to x- and y-axis of xyz system
P_x, P_y	Pitches of a 2D grating or lattice, and periods of its topographic signal $f(X,Y)$ in XYZ system
P_x, P_y	Projections of P_x and P_y in xoy plane: $P_x = P_x \cos \varphi_x$, $P_y = P_y \cos \varphi_y$
$\Delta x, \Delta y$	Scanning step sizes of an SPM in x- and y-axis
p_x, p_y	Computer-sampled data numbers within P_x and P_y periods
P_q, P_r	Periods of a half 2D sinusoidal waveform
$\Delta q, \Delta r$	Element intervals of a half 2D sinusoidal waveform
p_q, p_r	Element numbers within P_q and P_r periods

1. INTRODUCTION

The pitch described in this paper is the distance between adjacent similar structural features of one-dimensional (1D) and two-dimensional (2D) gratings and lattices on surfaces. In nanometer metrology and measurement, the International Organization for

Standardization (ISO) stipulates 1D and 2D gratings and lattices in several documents to calibrate diverse microscopes and instruments after metrologically verifying the pitch-related parameters, such as pitch average, pitch uniformity, etc. Microscopes and instruments include a family of scanning probe microscopes (SPM) [1], scanning electron microscopes (SEM) [2,3], various optical microscopes and contact stylus instruments that are used for areal surface roughness measurement [4,5]. Usually, metrological atomic force microscopes (AFM) and nano-measuring machines (NMM) [6-8] implement the metrological verification. This typically includes two steps: acquiring the three-coordinate topographic signal in raster-scan mode, and afterwards evaluating the pitch-related parameters according to a pitch evaluation method.

Beside the center-of-gravity (CG) method [9,10] and Fourier-transform-based (FT) method [10], another pitch evaluation method of 1D gratings based on a 1D correlation filter has been previously published [11,12]. A half 1D sinusoidal waveform sequence with period P_r is taken as a correlation filter. When it cross-correlates with a 1D grating topographic signal with period P , the noise can be greatly suppressed if $P_r \approx P$. After correlation filtering, the distance between any two adjacent waveform peaks, along the direction perpendicular to 1D grating lines, is one pitch. The method was described as the peak

detection (PD) method. The pitch average, uniformity and rotation angle around z-axis can be calculated using the PD-method.

It has always been cumbersome to evaluate the pitches of 2D gratings and lattices based on CG- and FT-methods. The 2D gratings and lattices (defined by XOY plane) are mounted on the stage (defined by xoy plane) of the measuring instrument to be subsequently raster-scanned into images. When raster-scanning only a cluster of 2D grating or lattice features into image, we will find that the grating and lattice structures are always orientating an unknown θ angle around z-axis relative to the xoy plane. The unknown θ angle, plus the accompanied noise, will make the CG- and FT-method performance more demanding and less correct. In order to avoid the θ angle, the strategy is to make sure that the θ angle in the xoy plane is minimized to zero ($\theta \approx 0^\circ$). To achieve this, the 2D grating or lattice that has been loaded onto the xoy plane, needs to be located, orientated, image-scanned and image-analyzed to determine if the raster-scan lines are parallel to any assumed line that passes through a series of gravity centers of the 2D grating or lattice. The above actions have to be iteratively repeated until $\theta \approx 0^\circ$. Regardless of the size, the raster-scan area is indispensable [13] for metrologically verifying a 2D grating or lattice on a metrological AFM or a NMM, as well as applying it as a standard material to metrologically calibrate an SPM [14], and to map its errors [15,16] in accordance with ISO standards [17]. Except for CG- and FT-methods, there is an absence of literature addressing the problem in 2D pitch evaluation methods. Therefore, our intention is to apply the PD-method to the pitch evaluation of 2D gratings and lattices by suppressing the noise and making the θ angle known, so that the CD- and FT-method can be precisely fulfilled with decreasing workload.

Commercially available software [18] has taken a unit cell of topographic signals from 2D gratings and lattices as the template to calculate the 2D correlation average. In this paper, a half 2D sinusoidal waveform is proposed as a template for all features of 2D gratings and lattices. It can achieve the equivalent impact and high credibility for analyzing the images and topographic signals containing repeated 3D structural features. Furthermore, the template as a CC filter can dramatically suppress the noise and greatly improve the signal-to-noise-ratio (SNR), consequently the positions and orientations of 3D features can be precisely characterized and measured.

For identifying positions and locations of the repeated structural features on diverse surfaces [19-22], others have applied a grayscale threshold segmentation to binarize images, and edge and centroid detection to extract the borders and locate the centers. In contrast, we will introduce the 2D CC filter and the peak detection based on local-maxima detecting and image processing for identifying the peak positions of 2D gratings and lattices. To the best of our knowledge, the binary and ternary image reconstruction procedure presented in the paper is unique. Finally, the mathematical explanation of the 2D CC filtering, as well as the practical algorithm to determine the periods of a 2D half sinusoidal waveform template have been annexed.

2. 2D SINUSOIDAL GRATING

A. Topographic and coexisted signals

When an SPM or a scanning tunneling microscope (STM) raster-scans a 2D sinusoidal grating along two orthogonal direction x and y at the step size Δx and Δy , it crosses the X - and Y -pitches, P_X and P_Y , of the 2D sinusoidal grating with an unknown θ angle. The raster-scanned 2D signal $F(x,y)$ (in such physical units as length, voltage, current, etc.), against the positions (x,y) can be decomposed as a 2D sinusoidal topographic signal $f(x,y)$, a nonlinear drift signal $U(x,y)$ and a noise signal $W(x,y)$, i.e.

$$F(x, y) = f(x, y) + U(x, y) + W(x, y) \quad (1)$$

Coordinate x and y , signal $F(x,y)$, $f(x,y)$, $U(x,y)$ and $W(x,y)$ are all $M \times N$ matrices in a raster-scan range $M\Delta x \times N\Delta y$. An example signal of a 2D sinusoidal grating with 300 nm nominal pitches, $F(x,y)$, is shown by a 2D intensity graph in Fig. 1(a).

It is supposed that the origin of XYZ coincides with that of xyz . Due to the existence of a 2D nonlinear drift signal $U(x,y)$, the XOY plane tilts a φ_x angle relative to x -axis and φ_y angle relative to y -axis. If the 2D sinusoidal topographic signal, in XYZ system is defined by

$$f(X, Y) = A \sin \frac{2\pi X}{P_X} \sin \frac{2\pi Y}{P_Y}. \quad (2)$$

It is expressed in xyz system as

$$\begin{aligned} f(x, y) &= A \sin \frac{2\pi(x \cos \theta - y \sin \theta)}{P_X \cos \varphi_x} \sin \frac{2\pi(x \sin \theta + y \cos \theta)}{P_Y \cos \varphi_y} \\ &= A \sin \frac{2\pi(x \cos \theta - y \sin \theta)}{P_x} \sin \frac{2\pi(x \sin \theta + y \cos \theta)}{P_y}, \end{aligned} \quad (3)$$

where, 1) $X=(x \cos \theta - y \sin \theta) / \cos \varphi_x$ and $Y=(x \sin \theta + y \cos \theta) / \cos \varphi_y$ means that the coordinates first rotate-transform by an θ angle from the XOY coordinates (of the 2D sinusoidal grating) to the xoy coordinates (of the measurement instrument), subsequently rotate-transform by φ_x angle around the x -axis and φ_y angle around the y -axis respectively; 2) The X - and Y -axes are parallel to the direction of the X -pitch and Y -pitch, P_X and P_Y , respectively; 3) $P_x = P_X \cos \varphi_x$ and $P_y = P_Y \cos \varphi_y$ mean the projections of P_X and P_Y in the xoy plane.

$U(x,y)$, according to ISO/DIS 11952[17], is presumably caused by piezo drift or creep in lateral or vertical direction; mechanical stresses of the sample holders and its fixers; mechanical expansion of the components such as measurement frame of an SPM. The diminishing effect on the accurate pitch evaluation can be leveled by rotation-transforming φ_x and φ_y angles around the x - and y -axis respectively, so that $U(X,Y) \approx 0$ in XYZ system, which means the drift signal theoretically does not exist in XYZ system. Mathematically, it is expressed by a 2D polynomial function in the xyz system whether it has been leveled or unleveled:

$$R_{tu}(x, y) = c + (a_1 x + b_1 y) + \dots + (a_K x + b_K y)^K. \quad (4)$$

where, $c = a_0 + b_0$ is the content item, a_i and b_i ($i=1,2, \dots, K$) are the coefficients of the i th order item of variable x and y , respectively.

$W(x,y)$ is given by the amplitude a_{xy} at any raster-scan position (x,y) :

$$W(x, y) = a_{x,y}. \quad (5)$$

B. 2D CC-filtered signals

A half 2D sinusoidal waveform template $T(q,r)$ with P_q and P_r periods is described by

$$T(q, r) = B \sin \frac{2\pi q}{P_q} \sin \frac{2\pi r}{P_r}. \quad (6)$$

$T(q,r)$ has a matrix of $M_T \times N_T$ elements against a matrix of $M_T \times N_T$ positions (q,r) with intervals Δq and Δr .

The correlation or convolution between $F(x,y)$ and $T(q,r)$ is expressed by

$$R_{TF}(x, y) = R_{TF}(x, y) + R_{TU}(x, y) + R_{TW}(x, y). \quad (7)$$

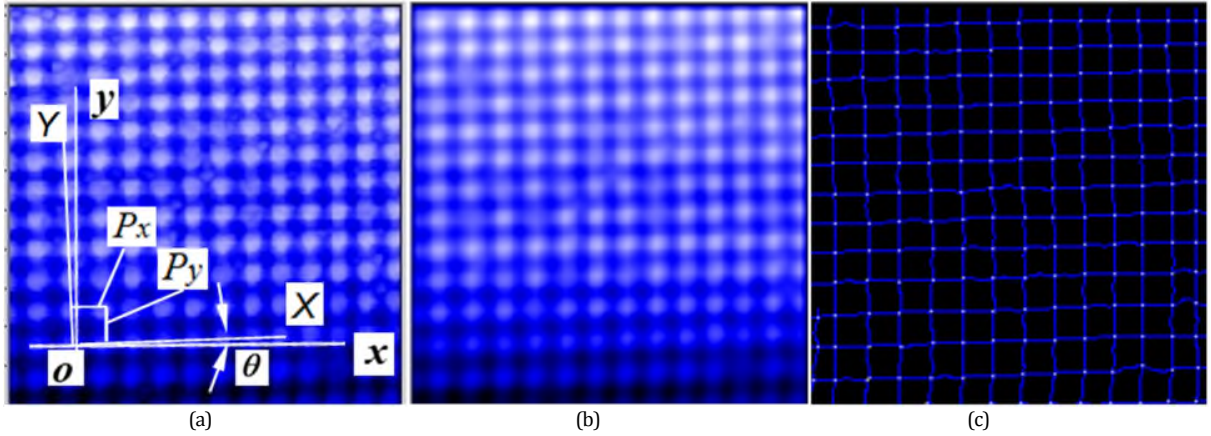


Fig. 1. (a), (b) and (c) shows 2D sinusoidal grating topographic signal $F(x,y)$, correlation-filtered signal $R_{TF}(x,y)$ and peaks detection image in intensity graphs, respectively.

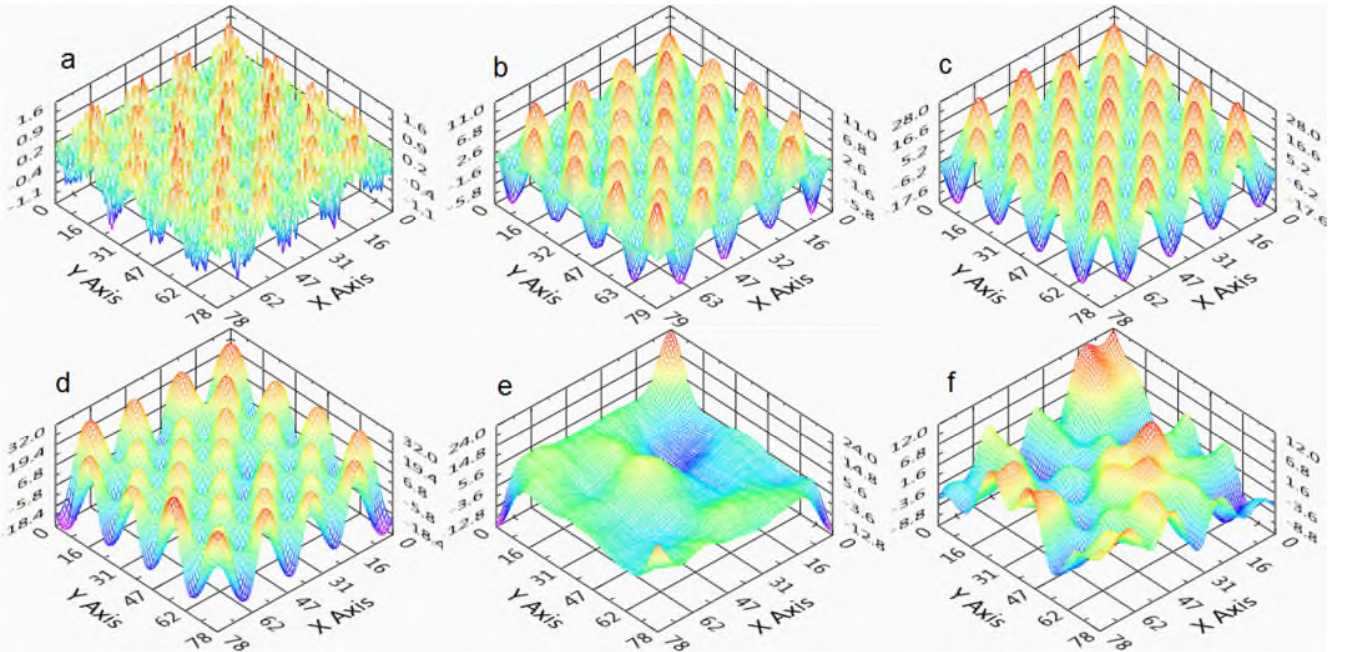


Fig.2. Based on convolution operation, 3D plots of filtered topographic signal $R_{TF}(x,y)$ (without normalization) with periods $P_x=P_y=20$ pixels; figure a, b, c, d, e and f are corresponding to $P_q=P_r=P/4, P/2, P, 2P, 3P$ and $4P$, respectively.

$R_{TF}(x,y)$, $R_{\eta}(x,y)$, $R_{\nu}(x,y)$ and $R_{\eta\nu}(x,y)$ are named as filtered signal, filtered topographic signal, filtered nonlinear drift signal and noise residue signal, respectively.

If correlation operator (+) and convolution operator (-) are combined into one operator (\pm), $R_{\eta}(x,y)$, $R_{\nu}(x,y)$ and $R_{\eta\nu}(x,y)$ in xyz system is developed as equation (8), (9) and (10), respectively. The mathematical developments are listed in **Annex A**.

$$R_{\eta}(x, y) = C[P_q]D[P_r] \sin\left(\frac{2\pi(x \cos \theta - y \sin \theta)}{P_x \cos \varphi_x} + \phi_x[P_q]\right) \cdot \sin\left(\frac{2\pi(x \sin \theta + y \cos \theta)}{P_y \cos \varphi_y} + \phi_y[P_r]\right). \quad (8)$$

$$R_{\nu}(x, y) = J + J_1(a_1x + b_1y) + \dots + J_K(a_Kx + b_Ky)^K. \quad (9)$$

$$R_{\eta\nu}(x, y) = \sum_{k=0}^{M_T-1} \sum_{l=0}^{N_T-1} A_{k,l} \cdot a_{(x \pm k \Delta q), (y \pm l \Delta r)}, \quad (10)$$

where $C[P_q]$ and $\phi_x[P_q]$ are concerned with P_q whilst $D[P_r]$ and $\phi_y[P_r]$ are related with P_r . They are defined by equation (A.3) ~ (A.6) in the Annex A. J is the constant item; J_1, J_2, \dots, J_K are the weighted index of monomial item, quadratic item, ..., and K th order item of the binary polynomials, respectively. They are explained by equation (A.8) ~ (A.10) in Annex A.

Compared with equation (3), equation (8) verifies that $R_{\eta}(x,y)$ remains a 2D sinusoidal signal. Its periods, P_x and P_y , are equal to the periods of $f(x,y)$, though the amplitude has changed to $C[P_q]D[P_r]$ and phases have shifted to $\phi_x[P_q]$ and $\phi_y[P_r]$.

Compared with equation (4), equation (9) interprets that $R_{\nu}(x,y)$ still is a nonlinear drift signal. It will not disturb the peaks detection even if it is unlevelled beforehand, or if it is not totally diminished after levelled.

In contrast to equation (5), equation (10) is the operation of weighted moving average (WMA) of the noise signal a_{xy} by using a matrix of data A_{kl} ($k=0, 1, \dots, M_T-1, l=0, 1, \dots, N_T-1$) as the weights. A_{kl} is expressed by equation (A.12) in Annex A.

Therefore, after correlation or convolution (CC) filtering, the noise signal a_{xy} , from highly dense irregularities, is minimized to a small and gently changing noise residue signal $R_{TW}(x,y)$. Although it can more or less modulate the amplitude of the $R_{TF}(x,y)$ if it is superimposed to the latter, it does not influence the periodicity of the latter (see Fig. 3 ref.[12]).

An 80×80 2D sinusoidal simulation signal $f(x,y)$ of 1 arbitrary unit (a.u.) amplitude and 20 a.u. periods ($P_x=P_y=20$), with Gaussian white noise $W(x,y)$ of 0.3 a.u. standard deviation, was taken as an example to demonstrate how $R_{TF}(x,y)$ varies with period Pq and Pr of a half 2D sinusoidal waveform template $T(q,r)$. $T(q,r)$ has 1 a.u. amplitude and $M_T \times N_T$ elements, where $M_T=Pq/2$, $N_T=Pr/2$. Based on convolution operation, the 3D plots of $R_{TF}(x,y)$ are shown in Fig. 2, where 3D plots marked by a, b, c, d, e and f correspond to $Pq=Pr=P/4, P/2, P, 2P, 3P$ and $4P$, which are 5, 10, 20, 40, 60 and 80 a.u., respectively.

From a half 1D sinusoidal waveform as 1D cross-correlation filter [11,12], when a half 2D sinusoidal waveform of Pq and Pr periods correlates or convolutes with the raster-scanned signal of a 2D sinusoidal grating of P_x and P_y periods with noise, we can deduce:

- (1) it can greatly filter noise if $Pq \approx P_x$ and $Pr \approx P_y$;
- (2) it cannot completely filter noise if $Pq \ll P_x$;
- (3) it can filter noise but severely modulate the amplitude of signal $R_{TF}(x,y)$ to make it impossible to distinguish $R_{TF}(x,y)$ from $R_{TW}(x,y)$ if $Pq \gg P_x$ and $Pr \gg P_y$.

Thus, instead of directly detecting the pitches from the raster-scanned signal $F(x,y)$, the filtered signal $R_{TF}(x,y)$ is validated for the pitch detection if we chose $Pq \approx P_x$ and $Pr \approx P_y$. For 2D sinusoidal grating signal $F(x,y)$ shown in Fig. 1(a), the correlation-filtered signal $R_{TF}(x,y)$ is exhibited in 2D intensity graph in Fig. 1(b). The practical algorithm on how to choose Pq and Pr to implement the CC filtering is attached in **Annex B**.

3. 2D LATTICES

A 2D lattice is a repetitive arrangement of 3D features, such as pillars, hills, holes, dimples, etc. The 3D convex type features have parallelogram (rectangle, square, diamond, etc.) or circle bottoms and the 3D concave type features have parallelogram or circle tops. Lattices are fabricated such that the features are arranged in square, rectangular, hexagonal and oblique array. The arrangement is in similarity to 2D solid crystalline lattices. Mathematically, they are described by different analytic functions inside and zero outside the 3D features.

A. Topographic signals

For a P_x - and P_y -pitch lattice with any 3D feature in square, rectangular, hexagonal, and oblique array, the raster-scanned topographic signal (with P_x - and P_y -periods) is defined as $f(x,y)$ inside the 2D waveforms and zero outside. A primitive unit cell with a bottom or top area A can be defined in the rectangular range $G\{-P_x/2 \leq x \leq P_x/2, -P_y/2 \leq y \leq P_y/2\}$ so that the 3D feature waveforms at the origin lies entirely within the primitive unit bottom or top, where x and y are two independent real variables in the whole feature array. The topographic signal of two exemplar square lattices with 3D central-symmetric features in parallelogram holes and hills is shown in Fig. 3(a) and (b), respectively.

The topographic signal of a lattice can be developed as a 2D Fourier series in complex exponential form:

$$f(x, y) = \sum_{I, J=-\infty}^{\infty} [A_{IJ} \cdot \exp[j(\omega_{xI} + \omega_{yJ})]]. \quad (11)$$

where, $\omega_{xI} = 2\pi I/P_x$ and $\omega_{yJ} = 2\pi J/P_y$ are the angular frequency in x - and y -axes, respectively; A_{IJ} is the Fourier transformation coefficient given by

$$A_{IJ} = \frac{1}{G} \iint_G f(x, y) \exp[-j(\omega_{xI} + \omega_{yJ})] dx dy, \quad (12)$$

$$(I, J = \pm 1, \pm 2, \dots).$$

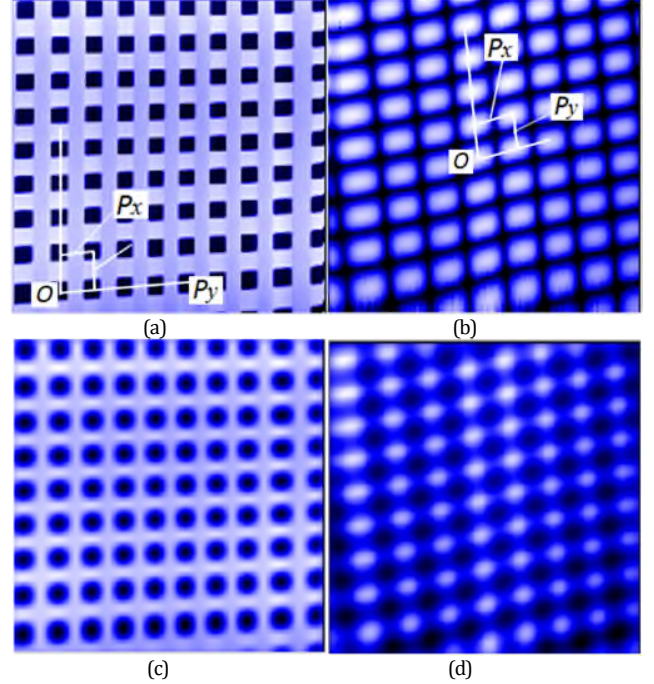


Fig. 3. Topographic signals of square lattices with 3D features in parallelogram holes and hills in (a) and (b); the correspondent correlation filtered signals are in (c) and (d) respectively.

To expand Equation (11) as the real form (**Annex C**), we find that 2D signal $f(x,y)$ consists of four group of 2D sinusoidal signals with different phase shifts in each group. Each group includes a constant item ($I, J=0$) and infinite numbers of 2D sinusoidal signals including a fundamental ($I, J=1$) period P_x and P_y , and harmonic period P_x/I and P_y/J ($I, J=2, 3, 4, \dots$). Since the amplitude A_{IJ} decreases sharply with I and J increasing [25], the sinusoidal waveform in fundamental period ($I, J=1$) dominates equation (11). Concerning the square lattices with such 3D central symmetric features as shown in Fig. 3 (a) and (b), equation (11) can be simplified as

$$f(x, y) = 4 \sum_{I, J=0}^{\infty} A_{IJ} \sin(\omega_{xI}x - \frac{\pi}{2}) \sin(\omega_{yJ}y - \frac{\pi}{2}) \quad (13)$$

B. 2D CC-filtered signals

If a half 2D sinusoidal waveform with period $Pq \approx P_x$ and $Pr \approx P_y$ is used to filter a series of 2D sinusoidal signals of 2D lattice (with periods P_x/I and P_y/J expressed by equation (13)). The filtered 2D sinusoidal signal with fundamental periods ($I, J=1$) has the same period P_x and P_y . The filtered 2D sinusoidal signals with harmonic periods, due to $Pq \gg P_x/I$ and $Pr \gg P_y/J$ ($I, J=2, 3, 4, \dots$), have been severely modulated. Moreover, with periods decreasing (i.e. I and J increasing), their amplitudes sharply dropped. Therefore, when the filtered 2D sinusoidal signals with fundamental and harmonic periods are combined into the filtered signal of 2D lattices, the filtered 2D sinusoidal signal in fundamental periods dominates.

The images of the 2D square holes and 2D hills in square arrays in Fig. 3 (a) and (b) are raster-scanned by different types of AFM in 256×256 pixels. The actual raster-scan ranges are 90μm×90μm and 50μm×50μm, respectively. After correlation-filtered using a half 2D sinusoidal waveform with periods, p_q and p_r of 30 pixels and 40 pixels, the filtered signals are plotted as 2D intensity graphs in Fig. 3 (c) and (d), respectively.

4. AUTOMATIC PEAK DETECTION

The peak detection in $R_{TF}(x,y)$ can be performed as follows. If a data $R_{TF}(m,n)$ at (m,n) ($m=0,1, \dots, M-1, n=0,1, \dots, N-1$) position in $M \times N$ matrix signal is the true peak, it is the local maximum in both row m and column n . First, two $M \times N$ zero matrices B_R and B_C are constructed. Based on the algorithm to find the local maxima in a sequence signals by applying quadratic/parabolic interpolation of three adjacent samples [23, 24], the following two steps are taken to detect the local maxima from row vectors and column vectors, respectively. Subsequently, the new values are assigned to the corresponding positions in B_R and B_C , respectively:

- (1) The local maxima of $R_{TF}(m,n)$ are detected row by row. If $R_{TF}(m,n)$ is detected as a local maximum in row m , $B_R(m,n)$ is converted to 1, otherwise it remains 0.
- (2) The local maxima of $R_{TF}(m,n)$ are detected column by column. If $R_{TF}(m,n)$ is detected as a local maximum in the column n , $B_C(m,n)$ is converted to 1, otherwise it remains 0.

As a result, B_R and B_C are dual-value $M \times N$ matrices. Apparently, $R_{TV}(x,y)$ and $R_{TW}(x,y)$ do not influence the local maxima detection, though they are included in $R_{TF}(x,y)$. If a data item $R_{TF}(m,n)$ is a true peak, it should be grey-scale 1 in both images, i.e. $B_R(m,n)=B_C(m,n)=1$. However, if it is only a local maxima, either $B_R(m,n)=1, B_C(m,n)=0$ or $B_R(m,n)=0, B_C(m,n)=1$. If B_R and B_C are merged into a new image G_E using logical 'AND' or arithmetical 'add' of the corresponding pixels, G_E consists of 0 and 1 or 0, 1 and 2 values. The former is called binary image and the latter is called ternary image. Those pixels with grey-scale 1 in the binary image G_E or grey-scale 2 in the ternary image G_E are the true peaks. Thus, a ternary images is displayed in dark background (grayscale=0), colored pixels (grayscale=1) and bright pixels (grayscale=2). The local maxima (grey-scale=1), which have disappeared in the binary image, can produce good visual effect in the ternary image to associate the peaks with the original and filtered images.

The peaks detection to the raster-scanned signal of the 2D sinusoidal grating in Fig. 1(a) is shown by the ternary image in Fig.1 (c). The peak detection of the signals in Fig.3 is shown in Fig. 4. Where, (a) and (b) are the ternary images before 2D correlation filtering. They appear chaotic and disordered due to noise; (c) and (d) are the ternary

images after 2D correlation filtering. The true peaks in bright pixels with grayscale 2 can be easily extracted from the ternary images Fig. 4 (c) and (d).

The peak detection process was applied to the raster-scanned signals of 2D atomic lattices: (1) silicon (111)-7×7 scanned by the variable temperature scanning tunneling microscope (VT STM) in 30nm×30 nm range and 800×800 pixel density shown in Fig. 5 (a); (2) HOPG scanned by the VT STM in 10nm ×10 nm range and 150×150 pixel density shown in Fig. 6 (a). As a result, the correlation-filtered signals ($p_q=p_r=30$ and 10 pixels, respectively) and the ternary images including true peaks and local maxima are shown in Fig. 5 (b) and (c) as well as Fig 6 (b) and (c), respectively. It is made possible to use atoms positions and unit cells to detect the directional drift of the sample, i.e., the motion of the scanner in an STM.

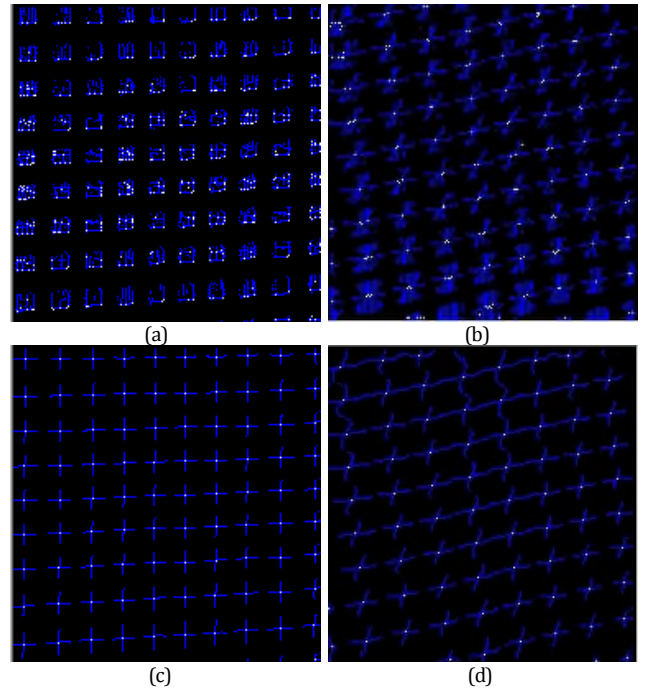


Fig. 4. Ternary image (a), (b), (c) and (d) are the peak detection results corresponding to the topographic signal (a) and (b), correlation filtered signal (c) and (d) in Fig. 3, respectively.

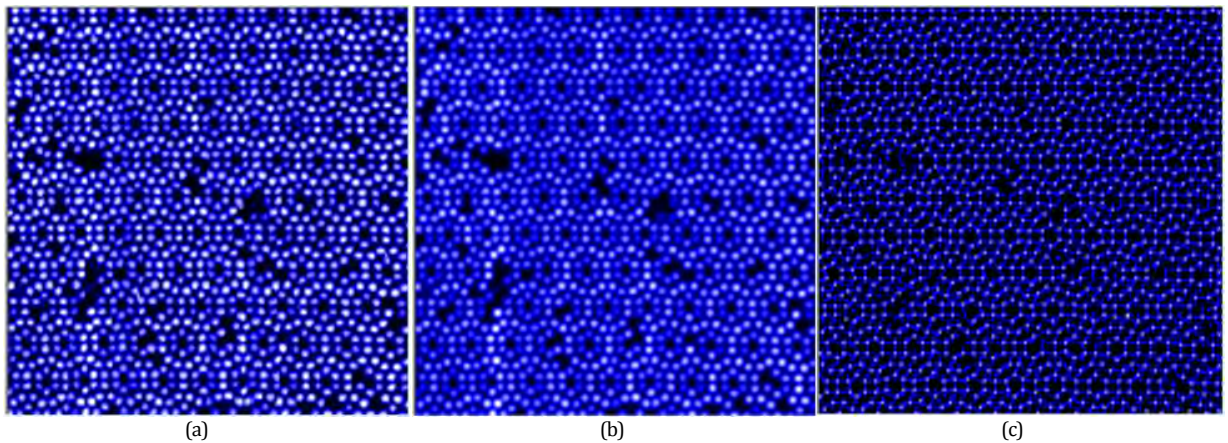


Fig. 5. Topographic signal of silicon (111)-7×7 (30 nm×30 nm scan-range, 800×800 pixel density) in (a), its correlation filtered signal in (b) and the peak detection ternary image in (c).

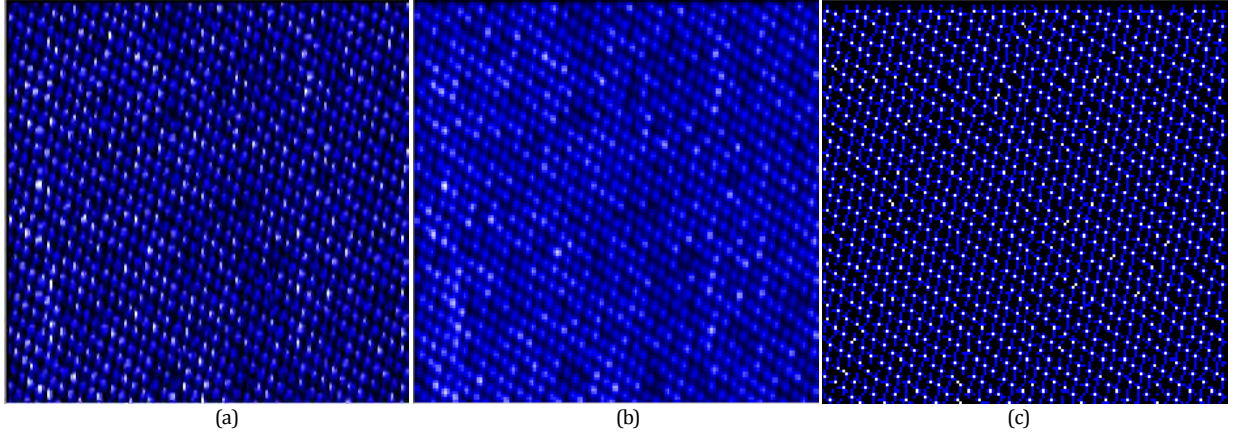


Fig. 6. Topographic signal of HOPG (10 nm×10 nm scan-range, 150×150 pixel density) in (a), its correlation filtered signal in (b) the peak detection ternary image in (c).

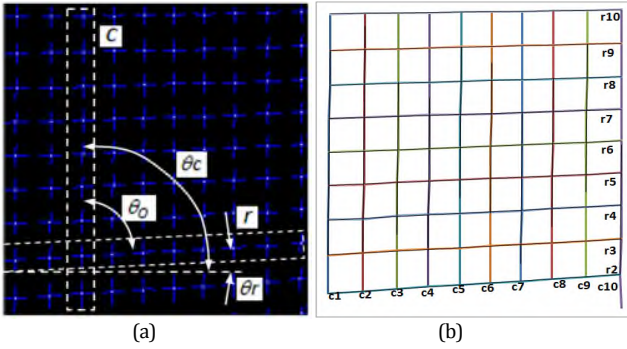


Fig. 7. Two narrow window, rotation angles θ_r and θ_c and orthogonal angle θ_o are schematically illustrated in the ternary image of the topographic signal of the 2D holes in (a); the correspondently fitted LSMLs are mapped in (b).

5. PITCH EVALUATION

If a pixel at (m,n) in a binary/ternary image is detected as true peak (grayscale=2), the correspondent computer-sampled position at (m,n) is (x,y) . If any two narrow windows are manually built, which enclose a line of peaks along P_x -direction and a line of peaks along P_y -direction, as demonstrated in Fig.7 (a), the peaks coordinates will be found to be $(x_1^{(r)}, y_1^{(r)})$, $(x_2^{(r)}, y_2^{(r)})$, $(x_3^{(r)}, y_3^{(r)})$, ..., $(x_K^{(r)}, y_K^{(r)})$ and $(x_1^{(c)}, y_1^{(c)})$, $(x_2^{(c)}, y_2^{(c)})$, $(x_3^{(c)}, y_3^{(c)})$, ..., $(x_L^{(c)}, y_L^{(c)})$ within the two narrow windows. The pitches are calculated by

$$\begin{cases} P_{xi}^{(r)} = [(x_i^{(r)} - x_{i-1}^{(r)})^2 + (y_i^{(r)} - y_{i-1}^{(r)})^2]^{1/2} \\ P_{yj}^{(c)} = [(x_j^{(c)} - x_{j-1}^{(c)})^2 + (y_j^{(c)} - y_{j-1}^{(c)})^2]^{1/2}, \end{cases} \quad (14)$$

$(i = 1, 2, \dots, K), (j = 1, 2, \dots, L)$.

In addition, one least-square mean line (LSML) r ($y=a_r x+b_r$) along P_x -direction and another LSML c ($y=a_c x+b_c$) along P_y -direction can be automatically fitted to two groups of peaks coordinates. Consequently, rotation angles θ_r and θ_c as well as orthogonal angle θ_o between the r and c can be determined by $\theta_r = \tan^{-1}(a_r)$, $\theta_c = \tan^{-1}(a_c)$ and $\theta_o = \theta_r - \theta_c$, respectively.

Moreover, LSML r_1, r_2, \dots, r_M and LSML c_1, c_2, \dots, c_N can be fitted to the peaks coordinates in a ternary image. For example, the ternary image of the 2D square holes in Fig. 7 (a) has nine LSMLs along P_x -direction and ten LSMLs along P_y -direction. They are mapped in Fig.7 (b).

If the pitches in a narrow window are evaluated as P_1, P_2, \dots, P_L (nm), the pitch average \bar{P} and uniformity δ can be automatically calculated using statistical mathematics.

6. PITCH EVALUATION RESULTS

PD-method is applied to the 2D grating in Fig.1 and two 2D lattices in Fig.3 for evaluating of pitch P_x and P_y , and related parameters. Before CC-filtering, three raster-scanned signals are leveled using the coordinate rotation-transformation to diminish the drift component $U(x,y)$, so as to make $P_x \approx P_y$ and $P_y \approx P_y$.

Table 1 Average of pitches \bar{P} , uniformity δ rotation angles $\bar{\theta}_c$ and $\bar{\theta}_r$, orthogonal angle $\bar{\theta}_o$, etc. evaluated by the PD-method.

2D lattices	2D holes		2D CCD		Hutley	
	unit	pixel	nm	pixel	nm	pixel
\bar{P}_x -PD	26.6	9351.6	31.4	6132.8	19.6	306.3
\bar{P}_y -PD	28.4	9984.4	28.2	5507.8	18.9	295.3
δ_x	1.4	492.2	1.9	371.1	1.0	15.6
δ_y	1.3	457.0	1.4	273.4	1.7	26.6
$\bar{\theta}_c$ (deg)	89.509		94.927		90.997	
$\bar{\theta}_r$ (deg)	2.242		11.982		1.649	
$\bar{\theta}_o$ (deg)	87.267		82.945		89.348	

After leveling, CC-filtering and peak detecting, the fitted LSML coefficients a_r and a_c of 2D gratings and lattices can be acquired. Thus, the averages of rotation angles $\bar{\theta}_c$ and $\bar{\theta}_r$ as well as orthogonal angle $\bar{\theta}_o$ are calculated from the average \bar{a}_c and \bar{a}_r .

The pitch averages \bar{P}_x -PD and \bar{P}_y -PD, uniformity δ_x and δ_y , averages of rotation angles $\bar{\theta}_c$ (deg) and $\bar{\theta}_r$ (deg), orthogonal angles $\bar{\theta}_o$, etc. are listed in table 1, where 2D holes, 2D CCD and Hutley represent 2D square holes in square array, 2D CCD array panel and 2D sinusoidal grating, respectively. The scale factors C_x and C_y , are determined by the ratio of raster-scan ranges (unit: nm) to image sizes (pixel) in x - and y -axis respectively, which are 90000/256 and 4000/256 (nm/pixel), respectively. The '2D holes' is a certified 2D pitch standard with verified pitch value $P_x=P_y=10030$ nm and expanded uncertainty ± 30 nm; the '2D CCD' has (6000×5000) nm² nominal area in unit cell; the 'Hutley' has nominal pitch values of 300nm.

From table 1 we have noticed that there exist the varying degrees of non-orthogonality between x - and y -axes, unequal pitch average \bar{P}_x and \bar{P}_y for 2D holes and Hutley, and dispersed individual pitch value P_x and P_y . It implicates that the three different AFMs that were used for raster-scanning three 2D gratings and lattices have unequal scale factor C_x and C_y , cross-talking between x - and y -scanners, and other geometrical errors described in [17]. Therefore, if an AFM is not metrologically calibrated and corrected with compensation, the raster-scanned images will exhibit severe aberrance and distortion as shown in fig. 3 (a) and (b).

7. COMPARISON OF PITCH EVALUATION METHOS

As two series of LSMLs (i.e., r_1, r_2, \dots, r_M and c_1, c_2, \dots, c_N) along the P_x - and P_y -directions can be fitted to the peaks coordinates in the ternary image based on PD-method, two groups of 1D topographic signal sequences of a 2D grating or lattice can be extracted along the series of LSMLs. Consequently, the CG- and FT- methods can be applied in two groups of 1D signal sequences to evaluate pitches. The inter-comparison of three pitch evaluation methods is realized about 2D gratings and lattices.

Table 2 Inter-comparison of pitch evaluation results among the PD-, CG- and FT-method.

2D lattices	2D holes		2D CCD		Hutley	
unit	pixel	nm	pixel	nm	pixel	nm
\bar{P}_x -PD	27.1	9511.7	30.9	6040.7	19.6	306.1
\bar{P}_x -CG	27.0	9484.4	30.9	6035.2	19.5	305.4
\bar{P}_x -FT	25.7	9023.4	30.7	5998.9	19.5	304.7
$\bar{\delta}_x$ -PD	1.9	671.9	1.8	343.2	1.0	16.3
$\bar{\delta}_x$ -CG	1.9	668.0	1.7	323.7	1.4	21.2
$\sigma \bar{P}_x$	0.8	274.4	0.1	22.7	0.1	0.7
\bar{P}_y -PD	28.7	10072.3	27.9	5449.2	18.9	295.7
\bar{P}_y -CG	28.5	10023.0	27.9	5449.2	19.0	296.4
\bar{P}_y -FT	27.6	9696.1	27.4	5348.3	18.9	295.4
$\bar{\delta}_y$ -PD	1.7	597.7	1.4	273.4	1.6	25.0
$\bar{\delta}_y$ -CG	1.6	555.5	1.4	276.7	2.1	32.2
$\sigma \bar{P}_y$	0.6	204.5	0.3	58.3	0.1	0.5

The results for inter-comparisons among PD-, CG- and FT-methods are listed in table 2: \bar{P}_x -PD and \bar{P}_y -PD, \bar{P}_x -CG and \bar{P}_y -CG, \bar{P}_x -FT and \bar{P}_y -FT represent two pitches averages using the PD-, CG and FT-method; $\sigma \bar{P}_x$ and $\sigma \bar{P}_y$ denote the standard deviation of two pitches evaluation results, which reflect how three pitch evaluation methods are in agreement with each other; the $\bar{\delta}_x$ and $\bar{\delta}_y$ are the averages of pitches' uniformities δx and δy .

From the comparison among pitch evaluation methods, it is concluded that:

- (1) The pitch averages evaluated by using the PD- and CG-methods are within one pixel difference from each other, and the pitch average evaluated using the FT-method are within one and half pixels difference from that evaluated using the PD- and CG-methods, whereas one pixel is proportional to three significantly different raster-scan step lengths in nanometers, which are 351.56, 195.31 and 15.62 (nm) respectively;
- (2) It should be emphasized here that the CG- and FT-methods deal with 1D topographic signal sequences along the two series of LSML. Any LSML does not completely cross through all the peaks detected by the PD-method within the corresponding

narrow window. Nevertheless, the PD-method truly deals with the 2D topographic signals of 2D gratings and lattices.

8. CONCLUSION

Mathematic analysis with 2D perspective has explicated that a half 2D sinusoidal waveform template can be used as a 2D correlation and convolution (CC) filter. When it correlates or convolutes with the topographic signal $f(x,y)$ of a 2D grating or lattice raster-scanned by an SPM, and if its periods P_q and P_r are approximately equal to that of the topographic signal, P_x and P_y , the coexisted noise $W(x,y)$ can be dramatically suppressed. The practical algorithm has interpreted how to determine its two periods so as to implement the 2D CC filtering. After CC filtering, the peaks can be acquired based on local-maxima detecting, followed by image processing. The pitch evaluation based on 2D CC filtering together with local-maxima detecting and image processing to detect peak positions is called peaks detection (PD) method. The PD-method will not be influenced by the unknown angles of 2D gratings and lattices rotating in-plane relatively to the stage of measuring instruments. The 2D nonlinear drafting signal $U(x,y)$ which are simultaneously generated in the raster-scan process will not interfere the CC filtering whether or not it is leveled using coordinate rotation-transformation. The CC filtering allows conveniently and reliably evaluating the local pitches, the average and uniformity of the pitches, rotation angle, orthogonal angle between two pitches of 2D gratings and lattices. It is an additional benefit to the precise pitch evaluation of 2D gratings and lattices.

ACKNOWLEDGEMENTS

We gratefully acknowledge the UK's Engineering and Physical Sciences Research Council (EPSRC) funding of the EPSRC Centre for Innovative Manufacturing in Advanced Metrology and Physikalisch-Technische Bundesanstalt (PTB) for the visiting fellowship support to the first author for doing this work.

ANNEX A: MATHEMATIC EXPLANATION OF CC FILTERING

To deduce the three items of correlation or convolution operation in equation (7), correlation operator (+) and convolution operator (-) are combined into one operator (\pm) in the following equation developments.

The filtered topographic signal $R_{\eta}(x,y)$ can be expressed and developed as:

$$\begin{aligned}
 R_{\eta}(X, Y) &= \frac{AB}{M\eta N\tau} \sum_{k=0}^{M_x-1} \sum_{l=0}^{N_y-1} T(k\Delta q, l\Delta r) f(X \pm k\Delta q, Y \pm l\Delta r) \\
 &= \frac{AB}{M\eta N\tau} \sum_{k=0}^{M_x-1} \sum_{l=0}^{N_y-1} \left[\sin \frac{2\pi k\Delta q}{P_q} \sin \frac{2\pi l\Delta r}{P_r} \sin \frac{2\pi(X \pm k\Delta q)}{P_x} \sin \frac{2\pi(Y \pm l\Delta r)}{P_y} \right] \\
 &= \frac{AB}{M\eta N\tau} \sum_{k=0}^{M_x-1} \left[\sin \frac{2\pi k\Delta q}{P_q} \sin \frac{2\pi(X \pm k\Delta q)}{P_x} \right] \sum_{l=0}^{N_y-1} \left[\sin \frac{2\pi l\Delta r}{P_r} \sin \frac{2\pi(Y \pm l\Delta r)}{P_y} \right]. \tag{A.1}
 \end{aligned}$$

To factorize and reintegrate equation (A.1), it is rewritten as

$$\begin{aligned}
 R_{\eta}(X, Y) &= (C_1[P_q] \sin \frac{2\pi X}{P_x} \pm C_2[P_q] \cos \frac{2\pi X}{P_x}) \\
 &\quad \cdot (D_1[P_r] \sin \frac{2\pi Y}{P_r} \pm D_2[P_r] \cos \frac{2\pi Y}{P_r}) \\
 &= C[P_q]D[P_r] \sin \left(\frac{2\pi X}{P_x} + \phi_x[P_q] \right) \sin \left(\frac{2\pi Y}{P_r} + \phi_y[P_r] \right), \tag{A.2}
 \end{aligned}$$

where,

$$\begin{cases} C_1[P_q] = \frac{A}{M_T} \sum_{k=0}^{M_T-1} \sin \frac{2\pi k \Delta q}{P_q} \cos \frac{2\pi k \Delta q}{P_x} \\ C_2[P_q] = \frac{A}{M_T} \sum_{k=0}^{M_T-1} \sin \frac{2\pi k \Delta q}{P_q} \sin \frac{2\pi k \Delta q}{P_x} \end{cases} \quad (\text{A.3})$$

$$\begin{cases} D_1[P_r] = \frac{B}{N_T} \sum_{l=0}^{N_T-1} \sin \frac{2\pi l \Delta r}{P_r} \cos \frac{2\pi l \Delta r}{P_y} \\ D_2[P_r] = \frac{B}{N_T} \sum_{l=0}^{N_T-1} \sin \frac{2\pi l \Delta r}{P_r} \sin \frac{2\pi l \Delta r}{P_y} \end{cases} \quad (\text{A.4})$$

$$\begin{cases} C[P_q] = (C_1^2[P_q] + C_2^2[P_q])^{\frac{1}{2}} \\ D[P_r] = (D_1^2[P_r] + D_2^2[P_r])^{\frac{1}{2}} \end{cases} \quad (\text{A.5})$$

$$\begin{cases} \phi_x[P_q] = \pm \tan^{-1} \left(\frac{C_2[P_q]}{C_1[P_q]} \right) \\ \phi_y[P_r] = \pm \tan^{-1} \left(\frac{D_2[P_r]}{D_1[P_r]} \right) \end{cases} \quad (\text{A.6})$$

To express equation (A.2) in xyz coordinate system, it is rewritten as

$$R_{Tf}(x, y) = C[P_q]D[P_r] \sin \left(\frac{2\pi(x \cos \theta - y \sin \theta)}{P_x \cos \phi_x} + \phi_x[P_q] \right) \cdot \sin \left(\frac{2\pi(x \sin \theta + y \cos \theta)}{P_y \cos \phi_y} + \phi_y[P_r] \right). \quad (\text{A.7})$$

The filtered nonlinear drift signal $R_{Tf}(x, y)$ can be expressed and developed as

$$R_{Tf}(x, y) = \frac{B}{N} \sum_{k=0}^{M_T-1} \sum_{l=0}^{N_T-1} \left\{ \left[\sin \frac{2\pi k \Delta u}{P_u} \sin \frac{2\pi l \Delta r}{P_v} \right] \cdot [a_0 + b_0 + (a_1 x \pm k \Delta u + b_1 y \pm l \Delta r) + \dots + (a_K x \pm k \Delta u + b_K y \pm l \Delta r)^K] \right\}. \quad (\text{A.8})$$

If $\alpha = \pm(k\Delta q + l\Delta r)$ and $\beta_j = \alpha_j x + b_j y$ are set, according to binomial theorem, $(\alpha + \beta)^i = \sum_{j=0}^i C_i^j \alpha^{i-j} \beta^j$, equation (A.8) is developed as

$$R_{Tf}(x, y) = J + J_1(a_1 x + b_1 y) + \dots + J_K(a_K x + b_K y)^K. \quad (\text{A.9})$$

The coefficients of each item J_i ($i=0, 1, 2, \dots, K$) in equation (A.9) is given by

$$J_i = \frac{B}{M_T N_T} \sum_{k=0}^{M_T-1} \sum_{l=0}^{N_T-1} \left(\sin \frac{2\pi k \Delta q}{P_q} \sin \frac{2\pi l \Delta r}{P_r} \cdot \sum_{j=0}^i C_i^j [\pm(k\Delta q + l\Delta r)]^{i-j} \right), \quad (\text{A.10})$$

where, $C_i^j = \frac{i(i-1)(i-2)\dots(i-j+1)}{j!}$, $i \geq j$, ($i, j=1, 2, \dots, K$), and

$$J = J_0(a_0 + b_0).$$

The noise residue signal $R_{Tf}(x, y)$ is factorized and reintegrated as

$$\begin{aligned} R_{Tf}(x, y) &= \frac{1}{M_T N_T} \sum_{k=0}^{M_T-1} \sum_{l=0}^{N_T-1} T(k\Delta q, l\Delta r) W(x \pm k\Delta q, y \pm l\Delta r) \\ &= \frac{B}{M} \sum_{k=0}^{M_T-1} \sum_{l=0}^{N_T-1} \sin \frac{2\pi k \Delta q}{P_q} \sin \frac{2\pi l \Delta r}{P_r} \cdot a_{(x \pm k\Delta q), (y \pm l\Delta r)} \end{aligned} \quad (\text{A.11})$$

if

$$A_{k, l} = \frac{B}{M_T N_T} \sin \frac{2\pi k \Delta q}{P_q} \sin \frac{2\pi l \Delta r}{P_r} \quad (\text{A.12})$$

is set, equation (A.11) is rewritten as

$$R_{Tf}(x, y) = \sum_{k=0}^{M_T-1} \sum_{l=0}^{N_T-1} A_{k, l} \cdot a_{(x \pm k\Delta q), (y \pm l\Delta r)}. \quad (\text{A.13})$$

ANNEX B: PRACTICAL ALGORITHM OF CC FILTERING

The algorithm is used for practically choosing the period P_q and P_r to implement the correlation or convolution between $T(q, r)$ and $F(x, y)$.

If the raster-scanning positions x and y as well as 2D signal $F(x, y)$ of a 2D grating or lattice (with pitch P_x and P_y) are computer-sampled at equal step size, $\Delta x = \Delta y$. x, y and $F(x, y)$ are all $M \times N$ matrices of data, i.e., $x = \Delta x, 2\Delta x, \dots, (M-1)\Delta x$ and $y = \Delta y, 2\Delta y, \dots, (N-1)\Delta y$. The indexed element $x(m, n)$, $y(m, n)$ and $F(m, n)$ ($m=0, 1, \dots, M-1$; $n=0, 1, \dots, N-1$) mean the sampled position and topographic data in row m and column n . Here, m and n do not mean actual physical-coordinate value [26]. If $F(x, y)$ is plotted in 2D intensity graph and 3D plot, it is plotted against indices (m, n) but not against actually computer-sampled position data.

If $x = m\Delta x$ ($m=0, 1, 2, \dots, M-1$), $y = n\Delta y$ ($n=0, 1, 2, \dots, N-1$), $P_x = p_x \Delta x$, $P_y = p_y \Delta y$ and $\Delta x = \Delta y$ are put into equation (3), $R_{Tf}(x, y)$ can be written in discrete form:

$$f(m, n) = A \sin \frac{2\pi(m \cos \theta - n \sin \theta)}{p_x} \sin \frac{2\pi(m \sin \theta + n \cos \theta)}{p_y}, \quad (\text{B.1})$$

where, digital p_x and p_y are the equivalents of the sampled data number within the period P_x and P_y of $f(x, y)$. As P_x and P_y are unknown parameters that need to be evaluated, p_x and p_y can be roughly estimated from the plotted 2D intensity graph of $F(x, y)$.

Likewise, if $q = k\Delta q$ ($k=0, 1, 2, \dots, M_T-1$), $r = l\Delta r$ ($l=0, 1, 2, \dots, N_T-1$), $P_q = p_q \Delta q$ and $P_r = p_r \Delta r$ are put into equation (5), $T(q, r)$ can be written in discrete form:

$$T(k, l) = B \sin \frac{2\pi k}{p_q} \cdot \sin \frac{2\pi l}{p_r}, \quad (\text{B.2})$$

where, digital p_q and p_r are the equivalents of the elements number within period P_q and P_r of $T(q, r)$. Thus, p_q and p_r can be chosen approximately equal to p_x and p_y , i.e. $p_q \approx p_x$ and $p_r \approx p_y$; the $T(k, l)$ elements numbers, M_T and N_T , can be calculated as $M_T = p_x/2$ and $N_T = p_y/2$. Consequently, the algorithm of the 2D CC filtering is implemented by

$$R_{TF}(m, n) = \sum_{k=0}^{M_T-1} \sum_{l=0}^{N_T-1} T(k, l) F(m \pm k, n \pm l). \quad (\text{B.3})$$

ANNEX C: EXPRESSION OF 2D SIGNAL OF LATTICES

To expand the topographic signal of a lattice expressed by equation (12) as the real form [25]:

$$\begin{aligned}
f(x, y) &= \sum_{l,j=0}^{\infty} [A_{l1} \cos(\omega_{lx}) \cos(\omega_{ly}) + A_{l2} \sin(\omega_{lx}) \cos(\omega_{ly}) \\
&\quad + A_{l3} \cos(\omega_{lx}) \sin(\omega_{ly}) + A_{l4} \sin(\omega_{lx}) \sin(\omega_{ly})] \\
&= \sum_{l,j=0}^{\infty} \sum_{i=1}^4 [A_{lji} \sin(\omega_{lx} + \phi_{xi}) \sin(\omega_{ly} + \phi_{yi})],
\end{aligned} \tag{C.1}$$

where, $\phi_{xj} = -\frac{\pi}{2}, 0, -\frac{\pi}{2}, 0$; $\phi_{yj} = -\frac{\pi}{2}, -\frac{\pi}{2}, 0, 0$, if $j=1, 2, 3, 4$ respectively; whilst A_{lji} is the Fourier transformation coefficient given by

$$\begin{cases}
A_{l1} = \frac{4}{G} \iint_G f(x, y) \cos(\omega_{lx}) \cos(\omega_{ly}) dx dy \\
A_{l2} = \frac{4}{G} \iint_G f(x, y) \sin(\omega_{lx}) \cos(\omega_{ly}) dx dy \\
A_{l3} = \frac{4}{G} \iint_G f(x, y) \cos(\omega_{lx}) \sin(\omega_{ly}) dx dy \\
A_{l4} = \frac{4}{G} \iint_G f(x, y) \sin(\omega_{lx}) \sin(\omega_{ly}) dx dy
\end{cases} \tag{C.2}$$

References

- ISO/DIS 18115-2 Surface chemical analysis – Scanning probe microscopy – Terms used in scanning –probe microscopy, International Organization for Standardization (2010).
- ISO 29301 Analytical transmission electron microscopy – Methods for calibrating image magnification by using reference materials having periodic structures, International Organization for Standardization (2010).
- H. Kwon, S. Y. Noh and N. W. Song, Development of the size calibration SOP for SEM measurement, Proc. SPIE **8819**, 88190J(2013).
- ISO 5436-1 Geometrical Product Specifications (GPS) –Surface texture: Profile method; Measurement standards –Part 1: Material measures. International Organization for Standardization (2001).
- ISO 25178-70: Geometrical product specifications (GPS) –Surface texture: Areal Part 70: Physical measurement standards (2011).
- G. Dai, F. Pohlenz, H.-U. Danzebrink, M. Xu, K. Hasche, and G. Wilkening, Metrological large range scanning probe microscope, Rev. Sci. Instrum. **75**, 962-970(2014).
- J. A. Kramar, R. Dixon and N G Orji, Scanning probe microscope dimensional metrology at NIST, Meas. Sci. Technol. **22**, 024001(2011).
- R. Leach, J. Claverley, C. Giusca, C. Jones, L. Nimishakavi, W. Sun, M. Tedaldi and A. Yacoot, Advances in engineering nanometrology at the national physical laboratory, Meas. Sci. Technol. **23**, 074002(2012).
- I. Misumi, S. Gonda, T. Kurosawa and K. Takamasu, Uncertainty in pitch measurements of one-dimensional grating standards using a nanometrological atomic force microscope, Meas. Sci. Technol. **14**, 463-471(2003).
- G. Dai, L. Koenders, F. Pohlenz, T. Dziomba and H.-U. Danzebrink, Accurate and traceable calibration of one-dimensional grating, Meas. Sci. Technol. **16**, 1241-1249 (2005).
- X. Chen, L. Koenders and F. Haertig, Real-time cross-correlation filtering of a one-dimensional grating position-encoded signal, Meas. Sci. Technol. **22**, 085105 (2011).
- X. Chen and L. Koenders, A novel pitch evaluation of one-dimensional gratings based on a cross-correlation filter, Meas. Sci. Technol. **25**, 044007(2014).
- G. Dai, F. Pohlenz, T. Dziomba, M. Xu, A. Diener, L. Koenders, and H.-U. Danzebrink, Accurate and traceable calibration of two-dimensional gratings, Meas. Sci. Technol. **18**, 415-421(2007).
- A. Yacoot, L. Koenders Recent developments in dimensional nanometrology using AFMs. Meas. Sci. Technol. **22**, 122001(2011).
- M. Xu, T. Dziomba, G. Dai and L. Koenders, Self-calibration of scanning probe microscope: mapping the errors of the instrument, Meas. Sci. Technol. **19**, 025105(2008).
- P. Klapetek, L. Picco, O. Payton, A. Yacoot and M. Miles, Error mapping of high-speed AFM systems, Meas. Sci. Technol. **24**, 025006(2003).
- ISO/DIS 11952 Surface chemical analysis – Scanning probe microscopy –Determination of geometric quantities using SPM: Calibration of measuring systems, International Organization for Standardization (2011).
- <http://www.imagemet.com/index.php?main=products&sub=modules&id=5>
- S. M. Bhandarkar, X. Luo, R. Daniels, E. W. Tollner, A Novel Approach to Detection, Localization and 3-D Reconstruction of Internal Defects in Hardwood Logs Using Computer Tomography, Pattern Anal. Applic, **9**, 155-175(2006).
- N. Senin, G. MacAulay, C. Giusca, R. K. Leach, On the characterisation of periodic patterns in tessellated surfaces, surf. Topogr.: Metrol. Prop. **2**, 025005(2014).
- X. Chen, A. Longstaff, S. Parkinson, A. Myers, A method for rapid detection and evaluation of position errors of patterns of small holes on complex curved and freeform surface, Intern. Prec. Eng. Manuf. **15**, 209-217(2014).
- J. Park, C. H. Shin, M. Kim, J. Kim, J. K. Park, J. S. Kim, C. S. Jun, Y. Yim, J. Lee, Exact and reliable overlay metrology in nanoscale semiconductor devices using an image processing method, J. Micro/Nanolith. MEMS MOEMS, **13**, 041409(2014).
- J. O. smith III, X. Serra, PARSHL: An analysis/synthesis program for non-harmonic sounds based on a sinusoidal representation, <https://ccrma.stanford.edu/STANM/stanms/stanm43/stanm43.pdf> (1985).
- Peak detection using LabVIEW and Measurement Studio (2012) <http://www.ni.com/white-paper/3770/en/>.
- A. Jeffrey, Mathematics for Engineers and Scientists, in: Sixth ed., Chapman & Hall/CRC press LLC, Boca Raton, USA (2000).
- R. C. Gonzalez and R. E. Woods, Digital Image Processing, Addison-Wesley (1992).

Correlation and convolution filtering and image processing for pitch evaluation of 2D micro- and nano-scale gratings and lattices

Chen, Xiaomei

2017-03-14

© 2017 Optical Society of America. One print or electronic copy may be made for personal use only. Systematic reproduction and distribution, duplication of any material in this paper for a fee or for commercial purposes, or modifications of the content of this paper are prohibited.

Xiaomei Chen, Ludger Koenders, and Simon Parkinson. Correlation and convolution filtering and image processing for pitch evaluation of 2D micro- and nano-scale gratings and lattices. *Applied Optics*, 2017, Volume 56, Issue 9, pp2434-2443

<https://dspace.lib.cranfield.ac.uk/handle/1826/11669>

Downloaded from CERES Research Repository, Cranfield University